AIAA JOURNAL
Vol. 39, No. 1, January 2001

Simulation of Turbulent Swirl Flow in an Axisymmetric Sudden Expansion

Baoyu Guo,* Tim A. G. Langrish,† and David F. Fletcher‡
University of Sydney, Sydney, New South Wales 2006, Australia

The numerical simulation of the turbulent flows in axisymmetric sudden expansions with inlet swirl is addressed, with the focus being on the unsteady flow behavior. Numerical simulations using the Reynolds-averaged Navier–Stokes equations closed via the k–ε turbulence model are presented. Results for an expansion ratio of 1.96 and a Reynolds number of 1×10^5 (at the inlet) are presented for a range of swirl numbers from 0 to 0.48. The precessing vortex core (PVC) and most of the features observed experimentally, including the precession direction, zero-frequency swirl number, and vortex breakdown have been predicted. The calculated precession frequency for the case of an expansion ratio of 1.96 is in close agreement with that reported in the literature. Moreover, a higher-order oscillation, in addition to the low-frequency PVC, has been predicted over a range of swirl numbers.

Nomenclature

D	=	diameter of downstream pipe
d	=	diameter of upstream (inlet) pipe
E	=	expansion ratio of diameter D/d
f	=	oscillation frequency
k	=	turbulent kinetic energy
L, l	=	length of pipes included in the simulation
M	=	jet momentum flux
P	=	Reynolds-averaged pressure normalized by inflow dynamic pressure
Q	=	volumetric flow rate
R	=	pipe radius
Re	=	Reynolds number at the inlet
S	=	swirl number
Sr	=	Strouhal number
t	=	time
U	=	Reynolds-averaged axial velocity component
U_i, U_o	=	bulk velocity at the inlet and exit
V, W	=	Reynolds-averaged velocity components
ε	=	turbulence dissipation rate
ρ	=	fluid density

Introduction

SWIRLING flows exiting from a circular duct of larger cross section are widely used in industry, especially in combustion systems, because of their ability to provide intensive mixing in a small volume. The precession phenomenon is also frequently observed in swirling flows, such as burners[1–5] and cyclone separators.[6] In these practical situations, fluid flows through a duct that suddenly increases in cross-sectional area. A simple sudden expansion geometry is representative of these applications, and the investigations of the flow within this model geometry have proved to be informative. In this study, we concern ourselves with the full range of swirl numbers from zero until vortex breakdown, rather than concentrating on the high swirl numbers present in many of the preceding applications. Such flows are of interest in the analysis of the performance of spray dryers.

Regarding the precessing vortex core (PVC) in an axisymmetric sudden expanson flow, the most relevant studies seem to be those of Hallett and Gunther[2] and Dellenback et al.[3] Experiments were performed by Hallett and Gunther[2] on swirling airflow in a sudden expansion, with an expansion ratio of 2.22, to study the effect of swirl intensity on flow and mixing. For the highest swirl tested, a central recirculation zone (or vortex breakdown) was formed, whereas at swirl intensities below the critical value required for central backflow, a precession of the flow was discovered. This precession was strongest and most regular for low swirl intensity, whereas at higher swirl intensity the motion became increasingly irregular, until the advent of vortex breakdown damped out the precession completely. In addition, the shedding of large irregular eddies from the step downstream of the throat was observed, with an estimated frequency being between 5 and 10 times that of the precession.

Regarding the PVC in a small expansion for low swirl intensities, the work of Dellenback et al.[3] presented relatively complete information. They made measurements in turbulent swirling flows through an abrupt axisymmetric expansion with an expansion ratio of 1.94 and examined the influence of the swirl number. The measurements of mean and rms velocities were performed in a water flow using a laser Doppler anemometer. In the upstream tube, the Reynolds number was varied from 3×10^4 to 1×10^5 and the swirl number from 0 to 1.2 (see Table 1). Dellenback et al. noted that the PVC occurs for low swirl levels and that the PVC precesses with the mean swirl for larger swirl numbers and against the mean swirl for low swirl numbers. The frequency information was converted to a set of Strouhal numbers ($f D^3/Q$), which are shown in Fig. 1.

The flowfield in some process equipment, such as a spray dryer, can also be represented by an expansion pipe flow. Experimental observations show that an unstable flowfield is one of the important causes of wall particle deposition problems in spray dryers.[7] Although there have been a number of experimental investigations of the precession phenomenon, the in-depth understanding of the underlining mechanism still remains inadequate.

Currently, computational fluid dynamics (CFD) codes suffer from the lack of proper validation in this area of engineering interest. Specifically, most of the computational works on swirling flows have been concerned with steady-state flows, whereas little progress has been achieved so far in the numerical simulation of the precession phenomenon. In our earlier work,[8,9] the self-sustained oscillations in the axisymmetric sudden expansion flows without entry swirl have been simulated using CFD. In the simulations, care was taken to construct a high-quality mesh, to choose high-order discretization schemes and robust equation solvers, and to ensure adequate convergence. The principal motivation of the current work is to further investigate the applicability of the computational procedures to swirling flows, as well as the possibility of suppressing the large-scale unsteadiness, so that wall particle deposition is minimized in spray dryers. A better description of this type of unsteady flow can now be given based on the current simulations.

Mathematical Model

Full solutions of the time-dependent Navier–Stokes equations via direct numerical simulation (DNS) are restricted to very low

Received 26 November 1999; revision received 14 June 2000; accepted for publication 14 June 2000.

*Research Student, Department of Chemical Engineering.
†Associate Professor, Department of Chemical Engineering.
‡Honorary Academic, Department of Chemical Engineering.

Table 1 Summary of flow regions[3]

$Re = 3 \times 10^4$	Remarks	$Re = 1 \times 10^5$
$0 < S < 0.18$	Vortex precesses in direction opposite to the mean swirl	$0 < S < 0.12$
$S \approx 0.18$	Precession frequency goes to zero	$S \approx 0.12$
$0.18 < S < 0.37$	Vortex precesses in same direction as the mean swirl	$0.12 < S < 0.40$
$S \approx 0.37$	PVC vanishes	$S \approx 0.40$
$0.37 < S < 0.50$	Bubble-type vortex breakdown	$0.40 < S < 0.57$
$S \approx 0.50$	Transition from recirculating bubble to strong on-axis tube of recirculating flow	$S \approx 0.57$
$S > 0.50$	Strong on-axis recirculation	$S > 0.57$

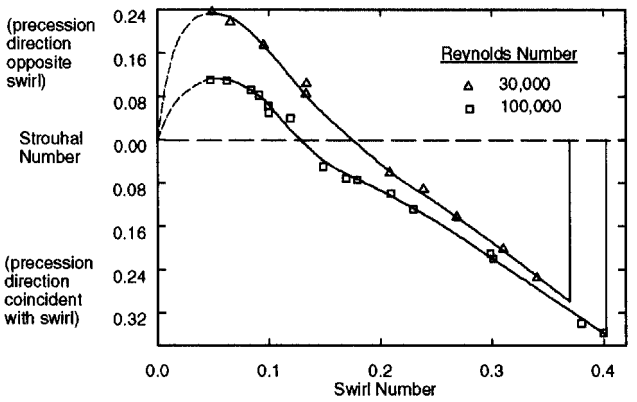

Fig. 1 Variation of Strouhal number with swirl number for flow in a sudden expansion with inlet swirl.[3]

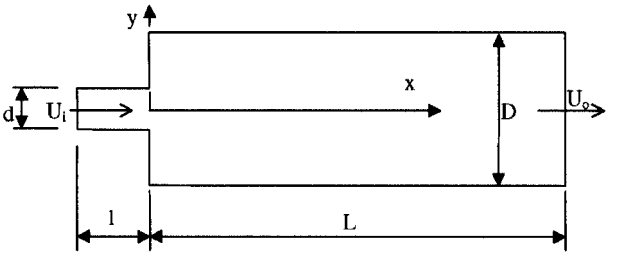

Fig. 2 Schematic diagram of the geometry used in the simulations.

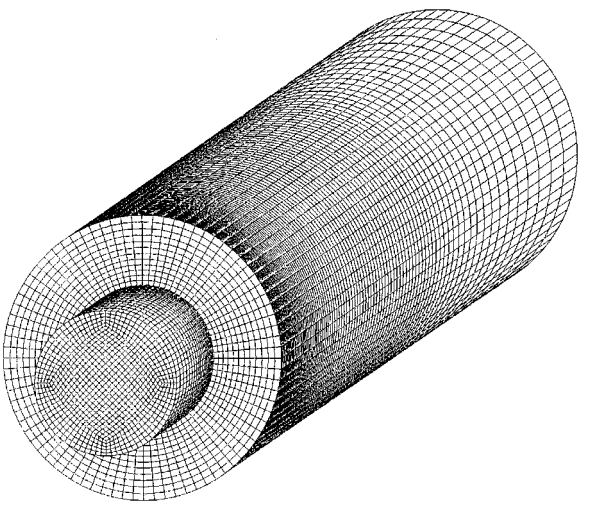

Fig. 3 Computational mesh used in the simulation with $E = 1.96$.

Reynolds numbers, and although large-eddy simulations (LES) are now competitive with DNS in accuracy at much lower cost, even LES is currently too expensive for routine calculations. Therefore, a Reynolds-averaging (time-averaging) method is usually used to solve for the mean quantities rather than for all details of the turbulence. In this case, a turbulence model has to be used to close the system of equations that addresses the unknown correlation terms of the velocity fluctuations (Reynolds stresses).

Detailed descriptions of turbulence models may be found in Ref. 10. The well-known k–ε model, with what has become known as the standard constants, has been used here, and convergence has been achieved readily. This model is more reliable with a high Reynolds number. It requires the use of either wall functions or viscous damping functions to calculate wall-bounded flows.

A previous study of self-sustained transient flow in a two-dimensional slab geometry has shown that the oscillatory behavior in this case was best reproduced using the standard k–ε model.[11] Simulations using a second-order closure model, the differential Reynolds stress model (DSM), gave results that, although fundamentally oscillatory, were unable to reproduce the well-defined oscillatory behavior obtained experimentally. We have, therefore, used the k–ε model in all later studies of transient flows of this type.

It is well known that for swirl flows the k–ε model predicts too rapid a decay of the swirl because it assumes an isotropic viscosity, when in fact the Reynolds stresses are highly anisotropic.[10] However, given the limitation of the DSM just described, the k–ε model was applied to this situation because it had already been shown to work well for two-dimensional[11] and three-dimensional[9] non-swirling flows. Therefore, note that the current simulations have a tendency to damp out instabilities due to the extra diffusion present.

Computational Model

The working fluid is specified as isothermal, incompressible, and Newtonian. For the purpose of direct comparison with the available experimental data, an axisymmetric sudden expansion configuration with an expansion ratio (diameter ratio) of $E = 1.96$ is investigated, which is close to that of Dellenback et al.[3] ($E = 1.94$) and of Hallett and Gunther[2] ($E = 2.22$). The geometry, coordinate system, and some of the notation are shown in Fig. 2. The inlet is located 5 diameters upstream from the expansion, and the downstream pipe is about 20 diameters long.

Swirling flows are usually categorized by the strength or degree of swirl (swirl number S), which is defined as the ratio of the axial flux of angular momentum to the axial flux of axial momentum divided by a characteristic radius. For a pipe with the coordinate axis on the centerline,

$$S = \frac{\int (yW - zV)U \, \mathrm{d}A}{R \int U^2 \, \mathrm{d}A} \tag{1}$$

where the x axis is on the centerline, R is the characteristic radius (the radius of the inlet is chosen in the current simulations), and $\mathrm{d}A$ is a differential element of area.

A uniform axial velocity profile is set and a swirl velocity is imparted to the flow at the inlet in the form of a solid body rotation (forced vortex). For the simple case with a uniform axial velocity and solid body type of swirl, Eq. (1) reduces to

$$S = \omega d / 4U_i \tag{2}$$

where ω is the angular velocity in the cross-stream plane. Based on the value of the axial velocity, the turbulence intensity at the inlet is set as 0.037, and the dissipation length scale is set to be the diameter of the upstream tube. These values are typical of those in a smooth pipe flow. At the exit, all quantities are treated as having no gradient in the streamwise direction, and the pressure reference is set at the center of the outlet. The log-layer solution is enforced for all walls to avoid the deficiency of the k–ε model in a wall boundary layer, as well as to avoid using a large number of grid points.

The computational mesh for this geometry is shown in Fig. 3, which is a fully three-dimensional, structured mesh with high orthogonality and smooth cell size variation. A higher cell density is applied in the proximity of the expansion to resolve the large flow gradient. The results were shown to be insensitive to the mesh, as described later in the paper.

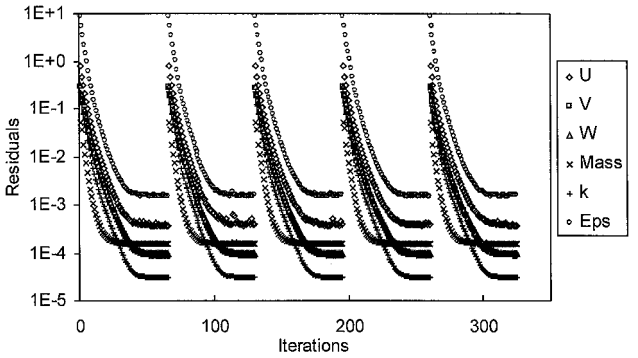

Fig. 4 Typical converged residual curves with each cycle corresponding to a time step.

Numerical Considerations

The simulations used the CFD program CFX4, which is based on a structured mesh and a finite volume formulation, to discretize the Navier–Stokes equations.[12] The differencing scheme used for the convective term is the third-order QUICK scheme[13] for all velocity components. The Van Leer scheme[14] is implemented for positive variables, such as the turbulence quantities k and ε. The PISO algorithm[15] was used for pressure correction. The quadratic (second-order), fully implicit scheme has been used for time differencing. A time step of around 0.01 s is small enough that the oscillation frequency is insensitive to further reduction. The linearized equation solvers used are Stone's method for velocities and algebraic multigrid for the pressure.

Usually a steady simulation is conducted at the initial stage, but it is extremely difficult to achieve a fully converged solution for the case of unstable flow. However, a global mass balance has been enforced, and residuals of other variables have been considerably reduced. A time-dependent calculation is then started from a steady calculation. Although the results appear to be chaotic and vary from case to case for an initial period of time after the time-dependent calculation is started, a reproducible time series of the flow variable is always produced. The initial period of time may be as long as 800 in terms of a dimensionless characteristic time defined in the next section. Moreover, the final solution is independent of the initial conditions.

As a convergence criterion, the sum of the absolute mass source residuals over all cells is less than 0.1% of the total flow rate. This procedure results in a sufficient number of iterations being carried out for each time step so that the residuals for all of the equations are consistently decreasing and approaching their limit of accuracy for single precision arithmetic. Figure 4 shows a typical set of well-converged curves for the residuals, where each cycle corresponds to a time step. (Because single precision numbers are used in the calculation, further reduction of the residuals is limited by the machine error.)

Time Variation of Flow Variables

During the simulation of a time-dependent problem, the values of the flow variables (velocity components, pressure, etc.) are recorded for each time step at some chosen monitoring points. The graphs presented here have been normalized into a dimensionless form. The velocity components have been normalized by U_i, and the pressure has been normalized by the dynamic pressure of the bulk flow at the inlet $\frac{1}{2}\rho U_i^2$. The time t is normalized as $U_i t/d$. To characterize the time variation of the flow, these time series are processed to give certain patterns, called limit cycles, which are obtained from the cross-stream velocity components V and W at fixed points on the geometric centerline. The limit cycle is a mathematical term that is sometimes used to describe the complicated behavior of nonlinear dynamical systems. Here it is used to facilitate the identification of the global motion of the flowfield.

Because the swirl boundary condition is implemented five diameters upstream of the expansion, the distribution of the flow variables changes before reaching the expansion throat. The results show that the swirl intensity decays within the entry tube. The angular momentum loss is 11–17%, and increases with increasing swirl in the range $S = 0.05$–0.6. Therefore, the values of swirl numbers in the rest of the paper are corrected so that they refer to the swirl numbers at the throat of the expansion, calculated according to Eq. (1). The angular momentum falls by about 54% in the downstream pipe over the length considered ($20D$), whereas this loss is about 40% in a simple swirling pipe flow. Consequently, the existence of an expansion has dissipated more swirl momentum compared with a swirl pipe flow.

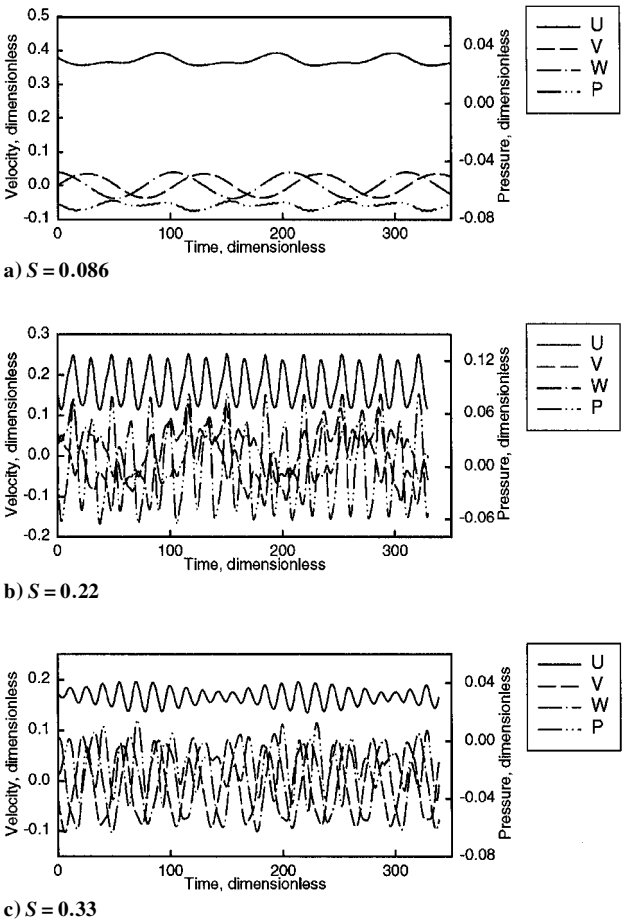

Fig. 5 Flow variables at the monitoring point $3D$ downstream from the expansion on the centerline ($E = 1.96$ and $Re = 1 \times 10^5$).

For the current expansion ratio of 1.96, the simulations show that any initial disturbances damp out and a steady solution is achieved for axial inlet flow conditions and for a range of swirl numbers less than 0.044. However, an increase in the swirl number above a critical value leads to a self-sustained precession. Figure 5 shows a time series of velocities and pressures monitored at a centerline point $3D$ downstream from the expansion for unsteady cases, and Fig. 6 shows limit cycles obtained $1D$ downstream from the expansion. Figures 5 and 6 show different behavior for different swirl numbers. For the case of $S = 0.086$, the monitoring point values show remarkable oscillations in velocities, which appear to be highly periodical, whereas the oscillation in pressure is relatively weak at the centerline point. The limit cycle is essentially circular, indicating that the precession is regular.

The precession is most regular at low swirl and becomes increasingly irregular as the swirl intensity increases. At a swirl number of 0.13, a higher-order oscillation arises that is one order of magnitude higher in frequency than, and superimposed on, a low-order precession. The motion of the flowfield becomes a combination of a low-frequency precession and a high-frequency oscillation in a rotating frame of reference corresponding to the low-frequency precession. Figure 5b is a time series of the flow variables for $S = 0.22$, which show a combination of two oscillations of different frequency. This high-order oscillation is sometimes found to behave like a precession because the limit cycle looks something like the orbit of the

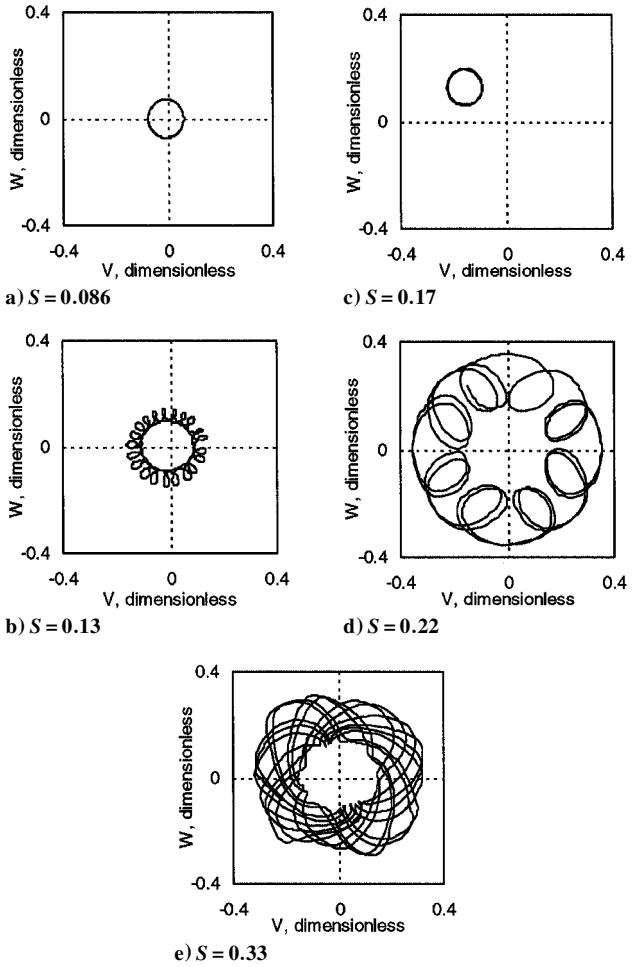

Fig. 6 Limit cycles for different swirl numbers at the centerline 1*D* from the expansion ($E = 1.96$ and $Re = 1 \times 10^5$): a) only the main PVC present, b) main PVC precesses in the opposite direction to the high-order precession, c) showing main PVC stops while the high-order precession is present, d) showing main PVC precesses in the same direction as the high-order precession, and e) showing bouncing-around pattern.

moon relative to the sun, that is, the vortex core is rotating around a point that is simultaneously moving around another fixed center point (as shown in Figs. 6b and 6d). The appearances of the limit cycles are different at different monitoring points. When proceeding downstream, the high-order precession evolves into a complex pattern along a path other than a circle, whereas the low-frequency precession remains fundamental throughout the domain. The amplitude of the higher-order precession is smaller than that of the lower-order one. Note that, although the high-order oscillation intensity in velocities is relatively weak, a strong pressure fluctuation results from the high-order oscillation.

The low-order precession almost stops when the swirl number is increased to 0.17 and reverses direction as the swirl number is further increased to 0.22, whereas the high-order precession remains in the same direction. At point $S = 0.17$, where the larger scale precession nearly stops, the limit cycles, as shown in Fig. 7, depart from the centerline, that is, become asymmetrical, and become more skewed downstream than upstream. However, the connecting line for the centers of the limit cycles, though not regular, display a spatially helical nature, which means that a high-frequency oscillation is moving around a three-dimensional curve. In other words, the flow pattern in this case can be interpreted as a combination of a steady asymmetric flow and an oscillation.

After the zero-frequency point, corresponding to $S = 0.17$, the frequency of the fundamental PVC increases linearly with the swirl number. When the swirl number is increased above 0.25, the high-order oscillation becomes weaker than the fundamental PVC. The high-order oscillation in the form of a precession is no longer evident, and the limit cycle displays a bouncing around pattern (Fig. 6e),

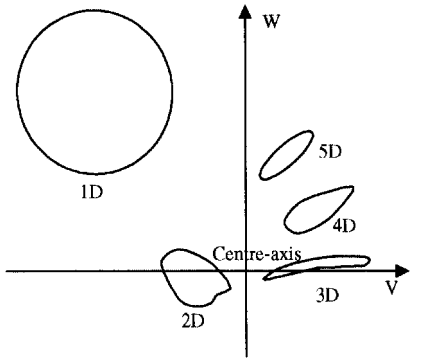

Fig. 7 Schematic diagram of limit cycles at different points downstream from the expansion ($E = 1.96$, $S = 0.17$, and $Re = 1 \times 10^5$).

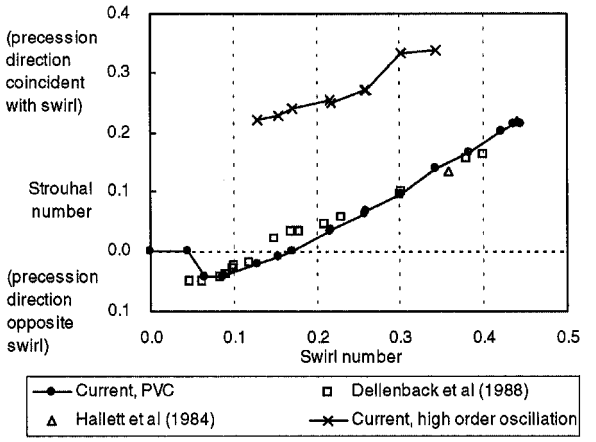

Fig. 8 Variation of Strouhal number with swirl number ($E = 1.96$ and $Re = 1 \times 10^5$); note excellent agreement between experimental data of Dellenback et al.[3] and current simulations.

that is, the vortex core constantly approaches the wall at an angle and is then pushed back.

With a further increase in the swirl strength to $S = 0.48$, a central recirculation bubble (referred to as vortex breakdown in the literature) occurs, and the flow simulation converges to a steady solution, suggesting that the precessions disappear altogether under this condition and that the breakdown serves to stabilize the flow. This is confirmed by the experimental observations of Hallett and Gunther[2] and Dellenback et al.[3]

Even though the large-scale oscillation is damped out, the turbulent kinetic energy is at a high level over the entire cross section of the chamber due to the shearing effect created by the central reverse flow. This implies that the intense mixing after the breakdown, as experienced in swirl burners, may be produced primarily by the small-scale turbulence rather than the large-scale flow entrainment. The steady state of the time-mean flowfield predicted after vortex breakdown is only restricted to a small expansion ratio considered in the current paper. However, this is not the case for a large expansion ratio of around five, as is reported in a later paper.[16]

Variation of Strouhal Number with Swirl Number

The characteristics of the PVC described by Dellenback et al.[3] (i.e., precession directions relative to the mean swirl, zero-frequency crossover, and vortex breakdown) have been predicted in the current simulations. The frequencies are normalized in terms of a Strouhal number

$$Sr = f\sqrt{\rho D^2}\,/\sqrt{M} \tag{3}$$

or

$$Sr = \left(2/\sqrt{\pi}\right)(fd/U_o) = \left(2/\sqrt{\pi}\right)E^2(fd/U_i) \tag{4}$$

The Strouhal number as a function of swirl number is shown in Fig. 8, with some reported data transcribed based on the current definition. The two curves for the current results represent the

frequencies for the decomposed precessions. Note that the low-frequency precession has a frequency of the same order as, and follows a general trend that is similar to, the experimental data of Hallett and Gunther[2] and Dellenback et al.[3] at comparable swirl intensities.

The limitations of the standard k–ε model are recognized,[10,17] and, consequently, it is essential to continue testing it against new experimental data. One of the limitations is that the model in many cases has proved to be over diffusive (giving too much mixing); therefore, the application of this model to the current problem would be likely to accelerate momentum transfer and damp out any oscillations. Nevertheless, this model, together with the current computational practice, performs well in capturing the fundamental features of the unsteady physical phenomenon and can predict an accurate frequency for the precessing vortex core. The weakness of the k–ε model may cause the oscillations, with the fluid moving downstream, to dissipate more quickly than in reality. This suggests that the instability is dominated by the near-field behavior close to the expansion and that the effect of the downstream flow is insignificant.

Significant deviation from the results of Dellenback et al.[3] occurs in only two regions, which were found by Dellenback et al. to be especially difficult to resolve experimentally. These are the precession frequencies for very low swirl ($S < 0.1$) and the swirl number at which the direction of precession changes. In the region of very low swirl, the simulated flow remains steady with a swirl number below a maximum value of about 0.044, whereas a smooth variation of the precession frequency with swirl number was implied in Fig. 1 by a dashed curved line. Apparently, the number of experimental data was inadequate to draw a firm conclusion.

In the other region, the calculated swirl number here is about 40% higher for the zero-frequency crossover, where the zero-frequency crossovers were obtained in the experiment by the interpolation of the swirl number. Because there was no experimental data point exactly at $Sr = 0$, the interpolated estimate in this case was probably sensitive to experimental errors. Regarding the onset of the vortex breakdown, the simulation gives a critical swirl number between 0.42 and 0.45, which is about 10% higher than that in the experiment. However, the transitional point has uncertainty because a hysteresis effect has been predicted.

For the high-order oscillation, the frequency is one order higher than the low-order precession and increases slightly with the swirl number. The corresponding Strouhal number is about 0.27. However, it is strongest within a range of swirl numbers from 0.13 to 0.21 and becomes weaker with increasing swirl when $S > 0.25$. Hallett and Gunther[2] observed the shedding of large eddies with a frequency between 5 and 10 times that of the PVC in their visualization. It appears that the high-order oscillation predicted here may be associated with the shedding of eddies because their frequencies are of the same order.

The Strouhal numbers presented by Dellenback et al.[3] show an appreciable difference between the Reynolds numbers from 3×10^4 to 1×10^5. In the simulation, however, the Reynolds number has no apparent influence on the Strouhal number for the same swirl number in the range considered here from 1×10^5 to 1.5×10^5. In view of the limitation of the turbulence model for low Reynolds numbers, we did not attempt a low Reynolds number simulation.

Visualization of the Flowfield

Figure 9 shows velocity vectors on a plane through the center axis of the pipes. For the steady state at a very low swirl number, the simulation result indicates that the reattachment to the wall occurs at approximately eight step heights downstream of the expansion, which agrees with the published results from many earlier studies.[18] For the high swirl number of 0.48, a central recirculation bubble occurs near the expansion throat (shown in Fig. 9c). The flowfield becomes steady and symmetric about the center axis. A central reversed flow occurs within a sphere-shaped space, which is located about 0.5 diameter downstream from the expansion and has a length scale of half of a pipe diameter. The axial velocity develops quickly to a uniform distribution after the breakdown bubble. The corner recirculation zone is considerably reduced in length to about 1.5 step heights.

For the moderate swirl numbers between 0.065 and 0.44, the flowfield has an instantaneously asymmetric pattern. Figure 10a is

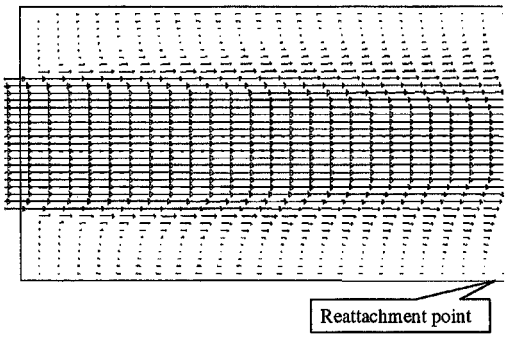

a) $S = 0$ (no swirl), showing steady symmetric

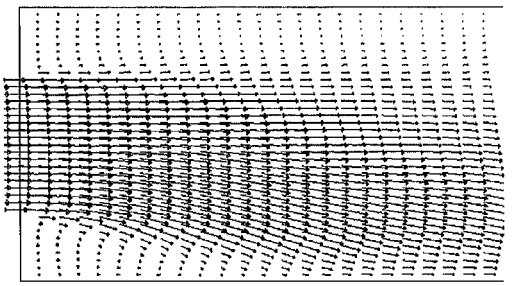

b) $S = 0.22$, showing instantaneously asymmetric flow pattern

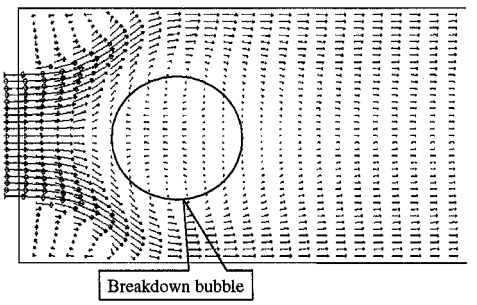

c) $S = 0.48$, showing a bubble vortex breakdown

Fig. 9 Vectors in a plane through the center axis ($E = 1.96$ and $Re = 1 \times 10^5$); note change in flow regime from a steady symmetric flow, through a transient flow, to a steady flow with vortex breakdown.

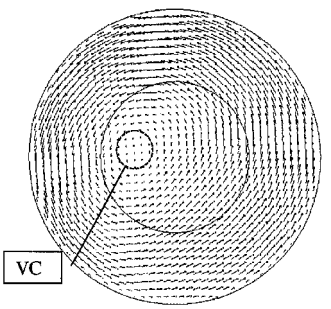

a) 5*D* downstream from the expansion

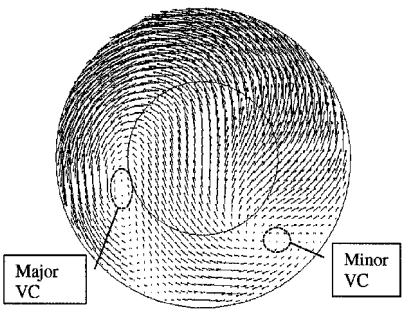

b) 3*D* downstream from the expansion

Fig. 10 Instantaneous velocity vectors showing biased vortex cores ($E = 1.96$, $S = 0.086$, and $Re = 1 \times 10^5$).

an instantaneous vector picture in a cross-sectional plane, showing a deflected vortex core for the case of $S = 0.086$. Although a well-defined vortex core can be identified clearly in most sections of the larger pipe, a minor vortex core occurs from around three to four diameters from the expansion, with the swirling direction being opposite to that of the major one (shown in Fig. 10b). The vortex cores deflect from the centerline by up to 30% of the diameter at $3D$ from the expansion, and this bias decreases as the flow proceeds farther downstream. Far downstream, the tangential velocity component in the pipe evolves toward a distribution similar to solid body rotation.

The spiral behavior of the PVC can be seen in an instantaneous isosurface of the velocity in Fig. 11. The curve connecting the vortex core is essentially parallel to the isosurface. The isosurface image of the velocity appears to be smooth and well defined for weak swirl and becomes increasingly complex with increasing swirl number. Some branches arise from the appearance of the high-order oscillations. At the zero-frequency point ($S = 0.17$), where the low-order precession stops, the high-order precessing axis (or three-dimensional vortex core) departs from the geometrical centerline and still displays a quasi-spiral shape. Because of the enhanced mixing caused by stronger swirl, the velocity gradient decreases with the swirl number until it becomes difficult to visualize the PVC above $S = 0.3$ with this technique.

Visualization of the instantaneous flowfield shows that, for the precession states, the vortex core always spirals in the same direction as the swirl and remains unchanged even when the precession reverses direction. The reason may be that any bias caused by a disturbance in a cross-sectional plane upstream would move downstream along the flow streamlines, which always have a spiral shape.

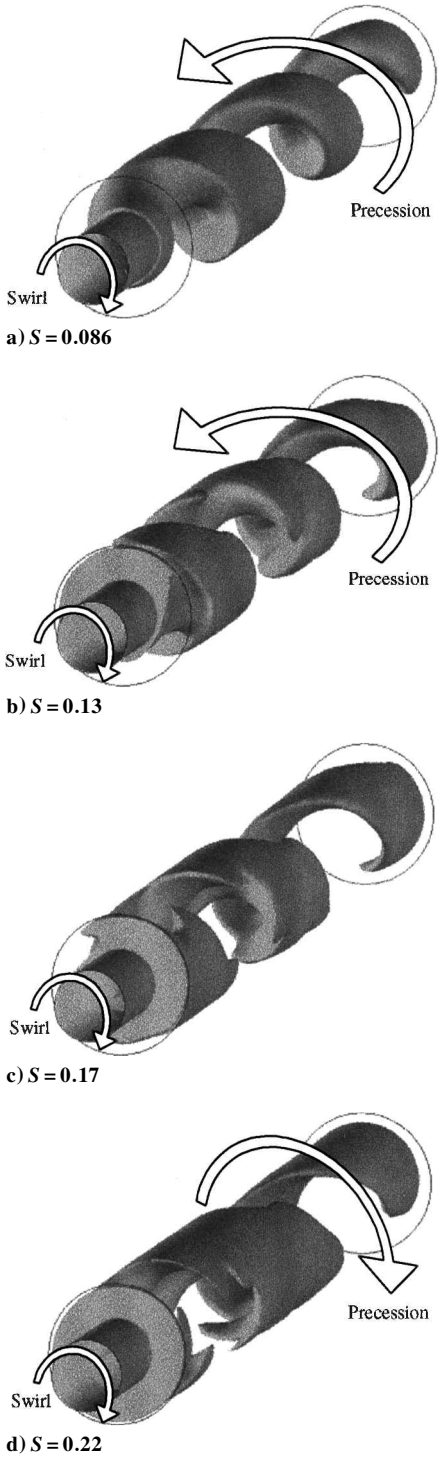

Fig. 11 Isosurfaces of velocity for different swirl numbers; note helical nature and increasing complexity as the swirl number increases, with the precession direction indicated relative to the swirling direction ($E = 1.96$ and $Re = 1 \times 10^5$).

Sensitivity Check

Sensitivity to Inlet Velocity Profiles

To investigate the effect of the inlet boundary conditions, a forced vortex swirl profile has been replaced in the simulation by a free vortex (with a forced vortex core), or, in another case, a fully developed pipe flow velocity profile has been used for the axial velocity. The presence of the precessions and frequencies are found to be insensitive to the actual shape of velocity profiles at the inlet. The inclusion of a length of tube within the solution domain upstream of the expansion allows any nonequilibrium values, specified at the inlet, to quickly develop toward realistic ones before the expansion. This removes any significant influence on the downstream flow.

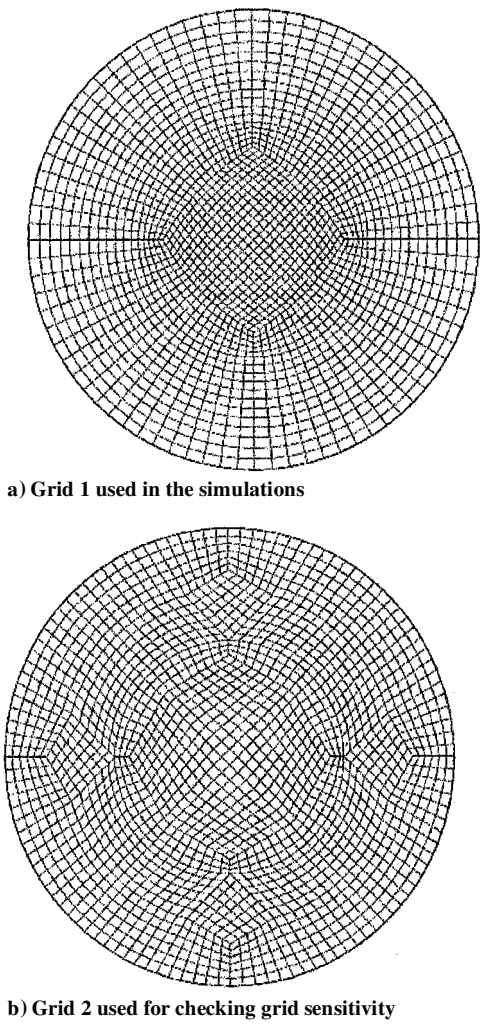

a) Grid 1 used in the simulations

b) Grid 2 used for checking grid sensitivity

Fig. 12 Cross-sectional view of the grids used in the simulations.

Grid Sensitivity

Figure 12 shows the cross-sectional view of the grids used. Most of the results have been achieved with grid 1, which consists of a total of 205,836 cells. Because all grid lines run through the central square, the cell density appears to be adequate at the central region. To make sure the simulation results are grid independent, another grid (grid 2) is generated, and the overall number of cells is increased by more than 30%. This finer grid differs from grid 1 in that the cell density is redistributed over the cross section, so that the cell density appears to be more uniform. The case of $S = 0.21$ has been chosen to examine the grid effect. A limit cycle pattern similar to that in Fig. 6d is reproduced, and the frequencies for both of the oscillations are within 2% of those for grid 1.

Conclusions

Simulation of turbulent swirling flows in axisymmetric sudden expansions has been carried out using CFD. Turbulence effects are represented by the standard k–ε model. The diameter expansion ratio is about 2:1, and the Reynolds number used is 1×10^5 based on the axial bulk velocity upstream. Entry swirl flow is prescribed with the swirl number from 0 to 0.48.

Imparting swirl causes the mean flow to become unstable and oscillatory. Precessing phenomena (precessing vortex core), which have been observed experimentally by other researchers, are predicted numerically in the current simulations. Most of the features, including the precession direction, zero-frequency swirl number, and vortex breakdown have been reproduced. The calculated precession frequency for the case of an expansion ratio of 1.96 is in close agreement with that reported by Hallett and Gunther[2] and Dellenback et al.[3] Moreover, a higher-order oscillation, in addition to the low-frequency PVC, has been predicted over a range of swirl numbers. Visualization shows that the flowfield has a helical nature.

The current simulation highlights a complex physical phenomenon for a simple fluid system in a simple geometric configuration and the capacity of the CFD approach to predict this class of problems. The computational model is based on an axisymmetric geometry with steady boundary conditions, indicating that the precessing vortex core is an inherent characteristic of the swirling flow inside the axisymmetric sudden expansion. The results also show that the standard k–ε model performs extremely well, as far as mean flow predictions are concerned, for this complex flow.

Acknowledgments

This work is supported by an Australian Research Council Large Grant. Helpful clarification by P. A. Dellenback, Department of Mechanical Engineering, University of Wyoming, regarding the Strouhal number and the measurements is appreciated.

References

[1]Gupta, A. K., Lilley, D. G., and Syred, N., *Swirl Flows*, Abacus, Tunbridge Wells, Kent, England, U.K., 1984, pp. 191–218.

[2]Hallett, W. L. H., and Gunther, R., "Flow and Mixing in Swirling Flow in a Sudden Expansion," *Canadian Journal of Mechanical Engineering*, Vol. 62, Feb. 1984, pp. 149–155.

[3]Dellenback, P. A., Metzger, D. E., and Neitzel, G. P., "Measurement in Turbulent Swirling Flow Through an Abrupt Axisymmetric Expansion," *AIAA Journal*, Vol. 26, No. 6, 1988, pp. 669–681.

[4]Nejad, A. S., and Ahmed, S. A., "Flow Field Characteristics of an Axisymmetric Sudden-Expansion Pipe Flow with Different Initial Swirl Distribution," *International Journal of Heat and Fluid Flow*, Vol. 13, No. 4, 1992, pp. 314–321.

[5]Fick, W., Syred, N., Griffiths, A. J., and O'Doherty, T., "Phase-Averaged Temperature Characterized in Swirl Burners," *Journal of Power and Energy*, Vol. 210, No. 5, 1996, pp. 383–395.

[6]Yazdabadi, P. A., Griffiths, A. J., and Syred, N., "Characterization of the PVC Phenomena in the Exhaust of a Cyclone Dust Separator," *Experiments in Fluids*, Vol. 17, No. 1/2, 1994, pp. 84–95.

[7]Southwell, D. B., and Langrish, T. A. G., "Observations of Flow Patterns in a Spray Dryer," *Drying Technology*, Vol. 18, No. 3, 2000, pp. 661–685.

[8]Guo, B., Langrish, T. A. G., and Fletcher, D. F., "Time-Dependent Simulation of Turbulent Flows in Axisymmetric Sudden Expansions," *Proceedings of 13th Australasian Fluid Mechanics Conference*, edited by M. C. Thompson and K. Howigan, Monash Univ., Melbourne, Australia, 1998, pp. 283–286.

[9]Guo, B., Langrish, T. A. G., and Fletcher, D. F., "Numerical Simulation of Unsteady Turbulent Flow in Axisymmetric Sudden Expansions," *Journal of Fluids Engineering* (submitted for publication).

[10]Wilcox, D. C., *Turbulence Modeling for CFD*, DCW Industries, Inc., La Cañada, CA, 1994, pp. 213–218.

[11]Guo, B., Langrish, T. A. G., and Fletcher, D. F., "An Assessment of Turbulence Models Applied to the Simulation of a Two-Dimensional Submerged Jet," *Applied Mathematical Modelling* (submitted for publication).

[12]*Solver Manual*, Harwell Lab., Didcot, Oxon, U.K., 1997, pp. 301–400.

[13]Leonard, B. P., "A Stable and Accurate Convective Modelling Procedure Based on Quadratic Upstream Interpolation," *Computer Methods in Applied Mechanics and Engineering*, Vol. 9, No. 1, 1979, pp. 59–98.

[14]Van Leer, B., "Towards the Ultimate Convective Difference Scheme. IV. A New Approach to Numerical Convection," *Journal of Computational Physics*, Vol. 23, No. 3, 1977, pp. 276–299.

[15]Issa, R. I., "Solution of the Implicitly Discretised Fluid Flow Equations by Operator Splitting," *Journal of Computational Physics*, Vol. 62, No. 1, 1985, pp. 40–65.

[16]Guo, B., Langrish, T. A. G., and Fletcher, D. F., "CFD Simulation of Precession in Sudden Pipe Expansion Flows with Low Inlet Swirl," *Applied Mathematical Modelling* (submitted for publication).

[17]Bradshaw, P., Launder, B. E., and Lumley, J. L., "Collaborative Testing of Turbulence Models," *Journal of Fluids Engineering*, Vol. 118, No. 2, 1996, pp. 243–247.

[18]Gould, R. D., Stevenson, W. H., and Thompson, H. D., "Investigation of Turbulent Transport in an Axisymmetric Sudden Expansion," *AIAA Journal*, Vol. 28, No. 2, 1990, pp. 276–283.

A. Plotkin
Associate Editor